Inorganic Chemistry

Article

pubs.acs.org/IC

Manganese/Cerium Clusters Spanning a Range of Oxidation Levels and $CeMn_8$, Ce_2Mn_4, and Ce_6Mn_4 Nuclearities: Structural, Magnetic, and EPR Properties

Christos Lampropoulos,[†] Annaliese E. Thuijs, Kylie J. Mitchell, Khalil A. Abboud, and George Christou*

Department of Chemistry, University of Florida, Gainesville, Florida 32611-7200, United States

Supporting Information

ABSTRACT: The syntheses, structures, and magnetic properties are reported for three new Ce/Mn clusters with different Ce/Mn ratios: $[Ce_6Mn_4O_{12}(O_2CMe)_{10}(NO_3)_4(py)_4]$ (py = pyridine) (**1**), $[CeMn_8O_8(O_2CCH_2{}^tBu)_{12}(DMF)_{14}]$ (DMF = dimethylformamide) (**2**), and $[Ce_2Mn_4O_2(O_2CMe)_6(NO_3)_4(hmp)_4]$ (**3**; hmp^- is the anion of 2-(hydroxymethyl)pyridine). **1** and **2** were obtained from the reaction of Ce^{IV} with $[Mn_{12}O_{12}(O_2CMe)_{16}(H_2O)_4]$ ($Mn^{III}{}_8Mn^{IV}{}_4$) and $[Mn_8O_2(O_2CCH_2{}^tBu)_{14}({}^tBuCH_2CO_2H)_4]$ ($Mn^{II}{}_6Mn^{III}{}_2$), respectively, whereas **3** resulted from the oxidation of Mn^{II} acetate with Ce^{IV} in the presence of hmpH. Cluster **1** possesses an unusual $[Ce_6Mn_4O_{12}]^{14+}$ core topology consisting of a $[Ce_6O_8]$ face-capped octahedron, which is face-fused at each end to a $[Ce^{IV}{}_2Mn^{III}Mn^{IV}O_4]$ cubane. Cluster **2** possesses a nonplanar, saddlelike loop of eight Mn^{III} atoms bridged by eight μ_3-O^{2-} ions to a central Ce^{IV} atom. Cluster **3** is similar to **1** in possessing an octahedral core, but this is now a $[Ce_2Mn_4]$ octahedron consisting of a Ce^{III} atom on either side of a Mn_4 parallelogram, with the metal atoms bridged by two μ_4-O^{2-} ions, the alkoxide arms of four hmp^- groups, and six acetates. Clusters **1**, **2**, and **3** are thus at the $Ce^{IV}{}_6Mn^{III}{}_2Mn^{IV}{}_2$, $Ce^{IV}Mn^{III}{}_8$, and $Ce^{III}{}_2Mn^{III}{}_4$ oxidation levels, respectively. Variable-temperature, solid-state direct current (DC) and alternating current (AC) magnetization studies on **1**−**3** in the 5.0−300 K range revealed predominantly antiferromagnetic exchange interactions within the complexes. For **1**, fitting of the DC data to the theoretical expression for a dinuclear $Mn^{III}Mn^{IV}$ complex derived using the Van Vleck equation and an isotropic spin Hamiltonian ($\mathcal{H} = -2J\hat{S}_i\cdot\hat{S}_j$ convention) gave a value for the exchange coupling parameter (J) of −60.4(7) cm^{-1} and a Landé factor g = 2.00(1), indicating an S = 1/2 ground state. For **2**, both DC and AC data indicate an S = 0 ground state, which is unprecedented for a member of the $CeMn_8$ family and now means members of the latter have been made that span the whole range of possible ground states from S = 0 to the maximum S = 16. Cluster **3** possesses an S = 0 ground state for its Mn_4 fragment, with the paramagnetism remaining at low temperature coming from the weakly coupled Ce^{III} centers. These three species are new additions to the Mn−Ce family of clusters and the broader class of 3d/4f molecular systems.

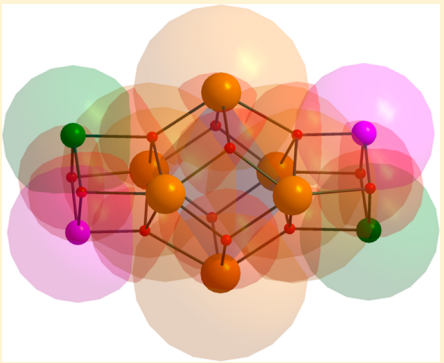

INTRODUCTION

Polynuclear 3d transition metal complexes have attracted a great deal of attention over recent years for a number of reasons, ranging from their complex and often aesthetically pleasing structures to the intriguing and even surprising physical properties that they sometimes display. For no 3d metal is the latter truer than for manganese and the unusual magnetic properties that it can exhibit. The molecular clusters of Mn containing at least some Mn^{III} display an amazing propensity to possess high ground-state spin (S) values. This is interesting in itself, but when coupled with significant easy-axis-type magnetoanisotropy (negative zero-field splitting parameter D), resulting from Mn^{III} Jahn−Teller axial elongations, such molecules may also be single-molecule magnets (SMMs), which are molecules able to function as single-domain nanoscale magnets below their blocking temperature T_B.[1] In addition, they can also display other fascinating properties such as quantum tunneling of magnetization (QTM)[2] and quantum phase interference.[3]

The incorporation of lanthanide (Ln) ions into Mn clusters to boost the anisotropy while hopefully still retaining the high spin of the Mn component has been one way that has been explored to enhance the properties of SMMs, and this approach has met with significant success, with examples being discovered with increased anisotropy barriers or still retaining the interesting quantum properties of the homometallic Mn SMMs, or both.[4−11] This interest in SMMs has also stimulated a broader interest into the development of new methods for the synthesis of 3d and mixed 3d/4f polynuclear clusters and their modification, as well as the identification and understanding of the origin of high ground-state spin values in molecular clusters in general, and the search for new types of cluster topologies.

Our own group's interest in Ln/Mn has not just concentrated on the use of the more anisotropic Ln ions, but also on Ce/Mn chemistry, and the present work is an extension of this interest. The ready availability and diamagnetism of the

Received: March 17, 2014
Published: June 6, 2014

   dx.doi.org/10.1021/ic500617f | Inorg. Chem. 2014, 53, 6805−6816

Table 1. Crystal Data and Structure Refinement Parameters for Complexes 1−3

	1·2py·6MeCN	2·$^3/_2$DMF	3·H_2O·6MeCN
formula[a]	$C_{62}H_{78}Ce_6Mn_4N_{16}O_{44}$	$C_{88.5}H_{170.5}CeMn_8N_{5.5}O_{37.5}$	$C_{48}H_{62}Ce_2Mn_4N_{14}O_{31}$
fw, g mol^{-1}	2811.88	2491.44	1831.12
space group	$P2_1/n$	$P\bar{1}$	$P\bar{1}$
a, Å	14.0419(2)	17.2684(11)	11.5998(9)
b, Å	14.3165(2)	17.5059(11)	12.0750(9)
c, Å	24.551(3)	23.2553(14)	13.1809(1)
α, deg	90	79.510(1)	108.886(1)
β, deg	104.253(2)	76.190(1)	104.727(1)
γ, deg	90	62.780(1)	90.137(1)
V, Å^3	4783.5(9)	6049.1(7)	1682.2(2)
Z	2	2	1
T, K	173(2)	173(2)	173(2)
radiation, Å[b]	0.710 73	0.710 73	0.710 73
ρ_{calc}, g cm^{-3}	1.952	1.368	1.808
μ, mm^{-1}	3.394	1.247	2.149
$R1$[c,d]	0.0717	0.0370	0.0341
$wR2$[e]	0.1795	0.0938	0.1009

[a]Including solvent molecules. [b]Graphite monochromator. [c]$I > 2\sigma(I)$. [d]$R1 = 100\Sigma(||F_o| - |F_c||)/\Sigma|F_o|$. [e]$wR2 = 100[\Sigma\ [w(F_o^2 - F_c^2)^2]/\Sigma[w(F_o^2)^2]]^{1/2}$, $w = 1/[\Sigma^2(F_o^2) + [(ap)^2 + bp]$, where $p = [\max(F_o^2, O) + 2F_c^2]/3$.

Ce^{IV} oxidation state makes it of little use for enhancing magnetic properties, and Ce^{III} is little better, and we have instead been stimulated to study this area by, among other things, the use of homo- and heterometallic Ce-containing compounds in inorganic, organic, environmental, and industrial applications owing to their ability to oxidize both inorganic and organic substrates.[12−18] Ce^{IV} is a strong oxidant and is, thus, used in a variety of catalytic systems, including the homogeneous and heterogeneous catalysis of water oxidation to molecular dioxygen by Ru complexes.[12a,b] In addition, Ce^{IV} is often used as the stoichiometric oxidant for the synthesis of Mn^{III}- and/or Mn^{IV}-containing compounds and mixed-valent $Co^{III,IV}$ complexes,[12,13,17] although usually without incorporating Ce in the product. Furthermore, Mn^{VII}, Mn^{IV}, and Ce^{IV} find extensive use in organic chemistry as oxidizing agents for a vast variety of organic substrates.[18] Their ability to act as heterogeneous catalysts has also been explored and yielded efficient catalysts for the de-NO_x catalysis of car exhaust gases.[19] Further, Ce^{IV}/Mn^{IV} composite oxides are widely used in sub- and supercritical catalytic wet oxidations for the treatment of wastewater containing toxic organic pollutants such as ammonia, acetic acid, pyridine, phenol, poly(ethylene glycol), and others.[15,16] For such reasons, we have also explored the use of Ce^{IV}/Mn^{IV} clusters in alcohol oxidation catalysis using O_2 as the oxidant.[20]

There are now a variety of Ce/Mn clusters in the literature since our initial reports of molecular Mn/Ce clusters over a decade ago.[8a,c] There have also been groups exploring the reactivity of Ce^{IV} with other 3d metals, and great effort has been invested in this chemistry both for a fundamental understanding of reactivity and for possible applications in homogeneous catalysis.[21] More recently, we have been investigating a variety of potential routes to new complexes, including the reaction of Ce-containing materials with preformed Mn_x clusters and organic chelates known to foster cluster formation. In this paper we report three new clusters from these efforts containing Ce_6Mn_4, $CeMn_8$, and Ce_2Mn_4 cores, two of which have particularly interesting structural features, and all three of which are noteworthy in some way.

EXPERIMENTAL SECTION

Synthesis. All manipulations were performed under aerobic conditions using chemicals as received, unless otherwise stated. $[Mn_{12}O_{12}(O_2CMe)_{16}(H_2O)_4]\cdot 2MeCO_2H\cdot 4H_2O$[22a] and $[Mn_8O_2(O_2CCH_2{}^tBu)_{14}({}^tBuCH_2CO_2H)_4]$[22b] were prepared as described elsewhere. Abbreviations: py = pyridine; hmpH = 2-(hydroxymethyl)-pyridine.

$[Ce_6Mn_4O_{12}(O_2CMe)_{10}(NO_3)_4(py)_4]$ (1). *Method A.* To a stirred solution of $[Mn_{12}O_{12}(O_2CMe)_{16}(H_2O)_4]$ (0.50 g, 0.25 mmol) in MeCN (20 mL) was slowly added solid $(NH_4)_2[Ce(NO_3)_6]$ (0.28 g, 0.50 mmol). The resulting solution was stirred for 30 min, during which time the color changed slightly from dark brown to red-brown. The solution was filtered, layered with pyridine (5 mL), and left undisturbed for 10 d at room temperature, during which time black needles of 1·2py·6MeCN slowly grew; the yield was 20% based on Ce. The crystals were maintained in mother liquor for the X-ray crystallographic analysis, collected by filtration, washed with Et_2O, and dried under vacuum for other solid-state studies. Selected IR data (KBr disk, cm^{-1}): 3437(m), 3162(m), 1618(w), 1539(s), 1401(vs), 1385(vs), 1211(w), 1116(w), 1070(w), 1018(w), 753(w) 671(b), 609(s), 530(s).

Method B. To a stirred solution of $[Mn_{12}O_{12}(O_2CMe)_{16}(H_2O)_4]$ (0.50 g, 0.25 mmol) in a solvent mixture comprising MeCN (15 mL) and pyridine (10 mL) was slowly added solid $(NH_4)_2[Ce(NO_3)_6]$ (0.28 g, 0.50 mmol). The resulting solution was stirred for 15 min, during which time the color changed slightly from dark brown to red-brown. The solution was filtered and left undisturbed for a period of 3 d, during which time black needles of 1·2py·6MeCN grew. They were isolated as for Method A; the yield was 40% based on Ce. The identity of the product was confirmed by elemental analysis, IR spectral comparison, and unit cell determination to be identical to material from Method A. Anal. Calcd (Found) for 1·4H_2O: C, 19.38 (19.79); H, 2.36 (2.77); N, 4.52 (4.47)%.

The picoline version $[Ce_6Mn_4O_{12}(O_2CMe)_{10}(NO_3)_4(pic)_4]$ (1′) can be obtained in comparable yield by the same method using picoline instead of pyridine. Anal. Calcd (Found) for 1′·2H_2O: C, 21.14 (21.25); H, 2.50 (2.75); N, 4.48 (4.26)%. It is significantly more soluble in common solvents than 1.

$[CeMn_8O_8(O_2CCH_2{}^tBu)_{12}(DMF)_{14}]$ (2). To a stirred solution of $[Mn_8O_2(O_2CCH_2{}^tBu)_{14}({}^tBuCH_2CO_2H)_4]$ (0.70 g, 0.25 mmol) in dimethylformamide (DMF) (30 mL) was slowly added solid $(NH_4)_2[Ce(NO_3)_6]$ (0.28 g, 0.50 mmol). The resulting solution was stirred for 30 min, during which time the color changed slightly from red-brown to dark brown. The solution was filtered and left

dx.doi.org/10.1021/ic500617f | Inorg. Chem. 2014, 53, 6805−6816

undisturbed for a period of 3 d, during which time black plates of $2\cdot{}^3/_2$DMF slowly grew; the yield was 40% based on Mn. The crystals were maintained in mother liquor for X-ray crystallographic analysis, collected by filtration, washed with Et_2O, and dried under vacuum for other solid-state studies. Anal. Calcd (Found) for **2** (solvent free): C, 45.01 (44.83); H, 7.19 (7.09); N, 2.50 (2.28)%. Selected IR data (KBr, cm^{-1}): 3446(mb), 2949(m), 1653(s), 1587(s), 1541(s), 1400(vs), 1306(m), 1242(m), 1104(m), 972(w), 903(w), 801(w), 731(s), 685(vs), 592(vs), 505(mb), 424(m).

$[Ce_2Mn_4O_2(O_2CMe)_6(NO_3)_4(hmp)_4]$ (3). To a stirred solution of $(NH_4)_2[Ce(NO_3)_6]$ (0.55 g, 1.0 mmol) in MeCN (20 mL) was added solid hmpH (0.10 mL, 1.0 mmol). After stirring for 5 min, solid $Mn(O_2CMe)_2\cdot 4H_2O$ (0.25 g, 1.0 mmol) was added. The resulting dark red-brown solution was stirred for an additional 5 min and then filtered, and the filtrate was left undisturbed to concentrate slowly by evaporation. After 5 d, dark brown crystals of $3\cdot H_2O\cdot 6MeCN$ were collected by filtration, washed with Et_2O, and dried under vacuum; the yield was 60% based on Mn. Anal. Calcd (Found) for $2\cdot 2H_2O$: C, 27.96 (28.21); H, 3.00 (2.95); N, 3.62 (3.69)%. Selected IR data (KBr, cm^{-1}): 3387(bm), 1613(sm), 1446(s), 1386(s), 1051(sm), 825(sw), 771(sm), 667(sm), 563(bm).

X-ray Crystallography. Data were collected on a Siemens Smart Platform equipped with a CCD area detector and a graphite monochromator utilizing Mo Kα radiation (λ = 0.710 73 Å). Suitable crystals of the complexes were attached to glass fibers using silicone grease and transferred to a goniostat where they were cooled to 173 K for data collection. An initial search of reciprocal space revealed a monoclinic cell for **1**·2py·6MeCN and a triclinic one for $2\cdot{}^3/_2$DMF and $3\cdot H_2O\cdot 6MeCN$; the choice of space groups $P2_1/n$ for **1**·2py·6MeCN and $P\bar{1}$ for $2\cdot{}^3/_2$DMF and $3\cdot H_2O\cdot 6MeCN$ was confirmed by the subsequent solution and refinement of the structures. Cell parameters were refined using up to 8192 reflections. A full sphere of data (1850 frames) was collected using the ω-scan method (0.3° frame width). The first 50 frames were remeasured at the end of data collection to monitor instrument and crystal stability (maximum correction on I was <1%). The structures were solved by direct methods in *SHELXTL6* and refined on F^2 using full-matrix least-squares cycles. The non-H atoms were refined anisotropically, whereas the H atoms (except for those of disordered solvents) were placed in ideal, calculated positions and refined as riding on their respective C atoms. Absorption corrections by integration were applied based on measured indexed crystal faces. Crystal data and structure refinement parameters for the three complexes are listed in Table 1.

For **1**·2py·6MeCN, the asymmetric unit consists of half a Ce_6Mn_4 cluster, one pyridine, two MeCN, and two half MeCN molecules, the latter located on or close to symmetry elements. A total of 567 parameters were included in the structure refinement using 25 901 reflections with $I > 2\sigma(I)$ to yield R_1 and wR_2 of 7.17 and 16.76%, respectively. For $2\cdot{}^3/_2$DMF, the asymmetric unit consists of a $CeMn_8$ cluster and 1.5 molecules of DMF. One DMF is in a general position with its O and H atoms disordered, and they were refined in two parts with each occupancy fixed at 50%. The half DMF molecule is disordered about an inversion center. A total of 1343 parameters were refined in the final cycle of refinement using 22 645 reflections with $I > 2\sigma(I)$ to yield R_1 and wR_2 of 3.70 and 9.38%, respectively. For $3\cdot H_2O\cdot 6MeCN$, the asymmetric unit consists of half a Ce_2Mn_4 cluster, half a water molecule, and three MeCN molecules. The latter were disordered and could not be modeled properly; thus, program SQUEEZE,[23] a part of the PLATON[24] package of crystallographic software,[25] was used to calculate the solvent disorder area and remove its contribution to the overall intensity data. The N3 ligand is half disordered, and there is a half water molecule associated with one part of the disorder. The N4 ligand is fully disordered and was refined in two parts with their site occupancies dependently refined. A total of 356 parameters were included in the structure refinement using 6631 reflections with $I > 2\sigma(I)$ to yield $R1$ and $wR2$ of 3.41 and 9.90%, respectively.

Other Studies. Infrared spectra were recorded in the solid state (KBr pellets) on a Nicolet Nexus 670 FTIR spectrometer in the 400–4000 cm^{-1} range. Elemental analyses (C, H, and N) were performed by the in-house facilities of the University of Florida Chemistry Department (**2** and **3**) and at Atlantic Microlabs (**1**). Variable-temperature direct current (DC) and alternating current (AC) magnetic susceptibility data were collected using a Quantum Design MPMS-XL SQUID susceptometer equipped with a 7 T magnet and operating in the 1.8–300 K range. Samples were embedded in eicosane to prevent torquing. Pascal's constants were used to estimate the diamagnetic correction, which was subtracted from the experimental susceptibility to give the molar paramagnetic susceptibility (χ_M). Electron paramagnetic resonance (EPR) measurements were recorded on a Bruker Elexsys E580 with a Bruker 4116DM. Data were collected in the 50 to 7050 G field range with the following parameters for **1**: temperature = 20 K, power = 3.17×10^{-1} mW, frequency = 9.483 GHz, modulation frequency = 100.00 kHz, modulation amplitude = 5.00 G, and gain = 60 dB.

RESULTS AND DISCUSSION

Syntheses. In previous reports from our group, we primarily employed two general methods for preparing Mn/Ce molecular clusters: (i) the oxidation of simple Mn^{II} salts by Ce^{IV} in aqueous or partially aqueous solution containing an excess of carboxylic acids, affording a variety of Ce^{IV}/Mn^{IV} products of various nuclearities as high as seven,[8a,b] and (ii) the oxidative reaction of preformed homovalent Mn^{III} compounds with Ce^{IV}, which afforded products such as $Ce^{IV}Mn^{III}{}_8$[8c,26,27] and $Ce^{III}{}_4Mn^{III}{}_{10}$.[6c] Both routes were used in the present work, with route (ii) employing two preformed Mn_x complexes of both higher nuclearity and higher and lower average (av) oxidation states than previously employed: $[Mn_{12}O_{12}(O_2CMe)_{16}(H_2O)_4]$ ($Mn^{III}{}_8Mn^{IV}{}_4$; av +3.33) and $[Mn_8O_2(O_2CCH_2{}^tBu)_{14}({}^tBuCH_2CO_2H)_4]$ ($Mn^{II}{}_6Mn^{III}{}_2$; av +2.25).

An initial success was $[Ce_6Mn_4O_{12}(O_2CMe)_{10}(NO_3)_4(py)_4]$ (**1**), obtained from the reaction of $(NH_4)_2[Ce(NO_3)_6]$ with $[Mn_{12}O_{12}(O_2CMe)_{16}(H_2O)_4]$ in a 2:1 (Ce/Mn = 2:12) ratio in MeCN followed by layering with pyridine (Method A of the Experimental Section). However, the yield was poor (20% based on Ce), and the product was contaminated with some brown powder of a side product. Although the desired crystals could be manually separated, an improved synthesis was targeted. With the identity of **1** established by X-ray crystallography, a superior synthesis giving a higher yield of pure product was developed using pyridine as cosolvent (Method B). Attempts to optimize the procedure further by increasing the amount of Ce gave mixtures of products that could not be separated. The formation of **1** is summarized in simplified form in eq 1. The reaction is clearly very complicated, ostensibly involving oxidation by Ce^{4+} of the Mn_{12} reagent (av $Mn^{3.33+}$) to the $Ce^{4+}{}_6Mn^{3+}{}_2Mn^{4+}{}_2$ product (av $Mn^{3.5+}$).

$$[Mn_{12}O_{12}(O_2CMe)_{16}(H_2O)_4] + 18Ce^{4+} + 12NO_3{}^- + 14MeCO_2{}^- + 12py + 19H_2O + 0.5O_2 \rightarrow 3[Ce_6Mn_4O_{12}(O_2CMe)_{10}(NO_3)_4(py)_4] + 46H^+ \quad (1)$$

However, the Mn is in large excess in the reaction, and the Ce^{4+} in the product has not changed its oxidation state, so it is likely the reaction proceeds by Ce^{4+} initiating disruption of the Mn_{12} compound followed by structural rearrangements to give **1** and other Mn-rich products. In addition, atmospheric O_2 was likely involved in preventing Ce^{III} formation, and eq 1 was balanced accordingly.

Similar considerations apply to the formation of $[CeMn_8O_8(O_2CCH_2{}^tBu)_{12}(DMF)_4]$ (**2**) from the reaction of the Mn_8

dx.doi.org/10.1021/ic500617f | Inorg. Chem. 2014, 53, 6805–6816

reagent with Ce^{IV}. The Ce/Mn reaction ratio of 1:4 gave the $CeMn_8$ product **2** in 40% isolated yield, involving a change from a $Mn^{2+}{}_6Mn^{3+}{}_2$ (av $Mn^{2.25+}$) reagent to a $Ce^{4+}Mn^{3+}{}_8$ product. The reaction is summarized in eq 2, where R = $CH_2{}^tBu$.

$$[Mn_8O_2(O_2CR)_{14}(RCO_2H)_4] + Ce^{4+} + 4DMF + 3H_2O + 1.5O_2 \rightarrow [CeMn_8O_8(O_2CR)_{12}(DMF)_4] + 6RCO_2H + 4H^+ \quad (2)$$

Again, it is interesting to note that although Ce^{4+} usually acts as an oxidizing agent for Mn^{2+}, the Ce is found in the product as Ce^{4+}, suggesting the involvement of O_2. Attempts to increase the yield of **2** by using a Ce/Mn ratio of 1:8 again gave mixtures, attesting to the complexity of these reaction systems. The use of $Ce(ClO_4)_4$ instead of $(NH_4)_2[Ce(NO_3)_6]$ also gave **2** in comparable yield. **2** is a new member of a known $Ce^{IV}Mn^{III}{}_8$ family, although previous examples were made by different procedures from the one used here.[8c,26,27]

$[Ce_2Mn_4O_2(O_2CMe)_6(NO_3)_4(hmp)_4]$ (**3**) differs from **1** and **2** in that it was obtained from a reaction system containing hmpH, a versatile bridging and chelating group upon deprotonation. The reaction of $(NH_4)_2[Ce(NO_3)_6]$, $Mn(O_2CMe)_2{\cdot}4H_2O$, and hmpH in a 1:1:1 ratio in MeCN gave a dark red-brown solution from which **3** was isolated in 60% yield. Its formation is summarized in eq 3. Again unlike **1** and **2**, product **3** contains Ce^{III} not Ce^{IV}, being $Ce^{III}{}_2Mn^{III}{}_4$.

$$4Mn^{2+} + 4Ce^{4+} + 4NO_3^- + 4hmpH + 6MeCO_2^- + 2H_2O \rightarrow [Ce_2Mn_4O_2(O_2CMe)_6(NO_3)_4(hmp)_4] + 2Ce^{3+} + 8H^+ \quad (3)$$

This is consistent with the Ce^{4+}/Mn^{2+} = 1:1 reaction ratio, but only half of the generated Ce^{III} is incorporated into the product. Since **3** contains bound nitrate ligands, we also carried out the reaction with $Ce(ClO_4)_4$ to target a different product but were unable to isolate a clean product for identification. We were also unable to isolate clean products when the carboxylate was changed to propionate or benzoate.

Description of Structures. A PovRay representation of centrosymmetric $[Ce_6Mn_4O_{12}(O_2CMe)_{10}(NO_3)_4(py)_4]$ (**1**) and a stereopair are presented in Figure 1, and the labeled $[Ce_6Mn_4O_{12}]$ core is shown in Figure 2. Selected interatomic distances and angles are listed in Table 2. Complex **1** contains a $[Ce^{IV}{}_6Mn^{III}{}_2Mn^{IV}{}_2O_{12}]^{14+}$ core containing a central Ce_6 octahedron whose eight faces are each capped by a μ_3-O^{2-} ion. Attached at opposite ends of this central $[Ce_6O_8]$ unit are two $[Mn^{III}Mn^{IV}(\mu_2\text{-}O^{2-})_2]$ planar units, whose Mn atoms each attach to a central oxide ion, making it μ_4 (O8, O10, and their symmetry partners), and whose μ_2-O^{2-} ions become μ_3 by attaching to a Ce atom (Ce2, Ce3, and their symmetry partners). As a result, the complete core can be described as a central $[Ce_6O_8]$ octahedron face-fused with two $[Mn_2Ce_2O_4]$ cubanes, one at each end. Peripheral ligation is provided by eight $\eta^1{:}\eta^1{:}\mu$ $MeCO_2^-$ groups (each bridging a CeMn pair), a terminal py on each Mn atom, and two chelating NO_3^- groups on each of the equatorial Ce atoms Ce1 and Ce1′. The crystallographic symmetry is C_i, and the virtual symmetry is C_{2h}. The Mn atoms are all distorted octahedra, and the Ce atoms are all eight-coordinate with square-antiprismatic geometry. The oxidation states of the Mn and Ce atoms, and the deprotonated nature of the O^{2-} ions, were confirmed by bond-valence sum (BVS) calculations (Tables 3 and 4, respectively).[28] Fortunately, there is no static disorder between the Mn^{III} and Mn^{IV} atoms in their similar environments, and, therefore, the expected Jahn–Teller (JT) elongations of Mn^{III} atoms Mn4 and Mn4′ are clearly visible along the O8–Mn4–N3 axes, with the axial bonds (Mn4–O8 = 2.256(7)Å and Mn4–N3 = 2.313(1)Å) being >0.3 Å longer than the rest (1.879(8)–1.954(9)Å).

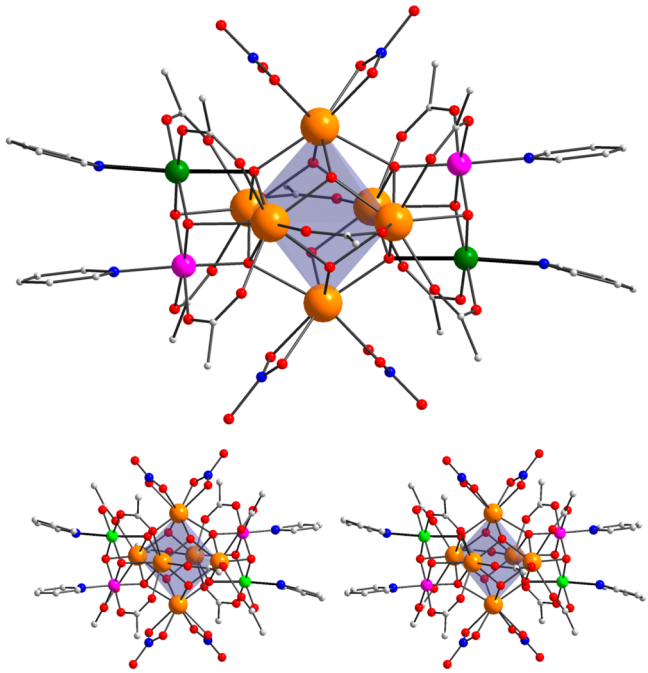

Figure 1. Structure and a stereopair of complex **1**. Thicker bonds denote Mn^{III} Jahn–Teller axes. Color code: Mn^{III} green, Mn^{IV} purple, Ce^{IV} orange, N blue, O red, C gray. H atoms are omitted for clarity.

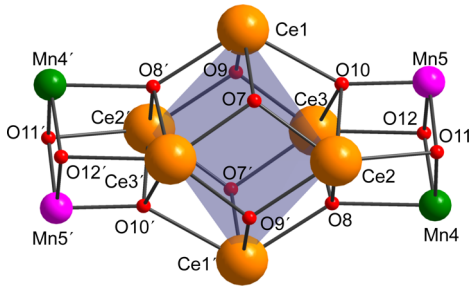

Figure 2. Labeled core of **1**; primed and unprimed atoms are related by the inversion center. Color code: Mn^{III} green, Mn^{IV} purple, Ce^{IV} orange, O red.

This is an unprecedented Mn/Ce topology, and to our knowledge is also unprecedented for any homo- or heterometallic cluster. The $[Ce_6O_8]$ octahedral unit has been previously reported, both by itself and with four or eight Mn^{III} atoms attached on the outside,[29] but these complexes are distinctly different from **1** in both the overall structure and its $Mn^{III/IV}$ oxidation level. The fusion of cubanes onto the central Ce_6 octahedron of **1** distorts the latter, as reflected in the range of Ce···Ce distances of 3.628(9)–3.800(10) Å, the shortest and longest being those between and within the cubanes, respectively. Inspection of the molecular packing reveals the presence of π–π stacking interactions between the two pyridine groups at each end, and between these and the pairs in

dx.doi.org/10.1021/ic500617f | Inorg. Chem. 2014, 53, 6805–6816

Table 2. Selected Interatomic Distances (Å) and Angles (deg) for Complex 1

Ce1···Ce3	3.667(1)	Ce2−O21	2.376(8)
Ce1···Ce3′	3.743(1)	Ce2−O14	2.383(9)
Ce1···Ce2	3.673(1)	Ce2−O16	2.387(9)
Ce1···Ce2′	3.744(1)	Ce2−O11	2.390(7)
Ce2···Mn5	3.269(2)	Ce3−O7	2.251(8)
Ce2···Mn4	3.368(2)	Ce3−O9	2.251(7)
Ce2···Ce3	3.800(1)	Ce3−O8	2.289(8)
Ce2···Ce3′	3.628(1)	Ce3−O22′	2.382(8)
Ce3···Mn5	3.277(2)	Ce3−O18	2.385(9)
Ce3···Mn4	3.371(2)	Ce3−O10	2.402(8)
Mn4···Mn5	2.809(3)	Ce3−O12	2.407(7)
Ce1−O9′	2.139(8)	Ce3−O20	2.414(9)
Ce1−O7	2.153(8)	Mn4−O12	1.879(8)
Ce1−O8	2.332(8)	Mn4−O11	1.885(8)
Ce1−O5	2.427(11)	Mn4−O13	1.943(9)
Ce1−O4	2.443(11)	Mn4−O17	1.954(9)
Ce1−O2	2.468(11)	Mn4−O8	2.256(7)
Ce1−O1	2.475(11)	Mn4−N3	2.313(10)
Ce1−O10′	2.506(8)	Mn5−O11	1.835(8)
Ce1−N2	2.816(2)	Mn5−O12	1.856(9)
Ce1−N1	2.880(16)	Mn5−O10	1.910(8)
Ce2−O7′	2.245(7)	Mn5−O15	1.948(9)
Ce2−O9′	2.280(8)	Mn5−O19	1.965(9)
Ce2−O8	2.340(8)	Mn5−N4	2.062(11)
Ce2−O10	2.372(8)		
Ce1−O7−Ce2′	116.7(3)	Mn4−O12−Ce3	103.0(3)
Ce1−O7−Ce3	112.7(3)	Mn5−O10−Ce3	98.2(3)
Ce2′−O7−Ce3	107.6(3)	Ce2−O10−Ce3	105.5(3)
Mn4−O8−Ce3	95.8(3)	Mn5−O10−Ce1′	149.4(4)
Mn4−O8−Ce1	145.5(4)	Ce2−O10−Ce1′	100.2(3)
Ce3−O8−Ce1	105.0(3)	Ce3−O10−Ce1′	99.4(3)
Mn4−O8−Ce2	94.2(3)	Mn5−O11−Mn4	98.0(4)
Ce3−O8−Ce2	110.4(3)	Mn5−O11−Ce2	100.6(3)
Ce1−O8−Ce2	103.7(3)	Mn4−O11−Ce2	103.4(3)
Ce1′−O9−Ce3	117.0(3)	Mn5−O12−Mn4	97.5(4)
Ce1′−O9−Ce2′	112.4(3)	Mn5−O12−Ce3	99.7(3)
Ce3−O9−Ce2′	106.4(3)	Mn4−O12−Ce3	103.0(3)
Mn5−O10−Ce2	99.0(3)		

Table 3. Bond Valence Sums and Assignments for Ce and Mn Atoms in 1−3

	atom	Ce^{III}	Ce^{IV}	atom	Mn^{II}	Mn^{III}	Mn^{IV}
1	Ce1	4.31	3.80[a]	Mn4	3.79	2.90	3.04
	Ce2	4.29	3.78	Mn5	3.93	3.59	3.77
	Ce3	4.30	3.79				
2	Ce	4.33	3.81	Mn1	3.20	2.93	3.07
				Mn2	3.19	2.91	3.06
				Mn3	3.22	2.95	3.06
				Mn4	3.16	2.89	3.04
				Mn5	3.21	2.94	3.09
				Mn6	3.17	2.90	3.04
				Mn7	3.23	2.95	3.10
				Mn8	3.18	2.91	3.05
3	Ce	2.99	2.63	Mn1	3.16	2.89	3.04
				Mn2	3.17	2.90	3.04

[a]The underlined value is the one closest to the charge for which it was calculated. The oxidation state can be taken as the nearest whole number to the underlined value.

Table 4. Bond Valence Sums and Assignments for the O Atoms[a] in 1 and 2

	atom	BVS	assignment
1	O7	2.01	O^{2-}
	O9	1.98	O^{2-}
	O11	1.83	O^{2-}
	O12	1.78	O^{2-}
2	O1	1.91	O^{2-}
	O2	1.78	O^{2-}
	O3	1.76	O^{2-}
	O4	1.95	O^{2-}
	O5	1.93	O^{2-}
	O6	1.79	O^{2-}
	O7	1.79	O^{2-}
	O8	1.93	O^{2-}

[a]An O BVS in the ∼1.8−2.0, ∼1.0−1.2, and ∼0.2−0.4 ranges is indicative of non, single, and double protonation, respectively.

neighboring molecules (C−C interpyridine distances ∼3.5−3.6 Å), giving sheets containing alternating chains of Ce_6Mn_4 molecules and π-stacked pyridine groups (Figure S1 of Supporting Information).[30]

A PovRay representation of $[CeMn_8O_8(O_2CR)_{12}(DMF)_4]$ (**2**) and a stereopair are presented in Figure 3, and its labeled

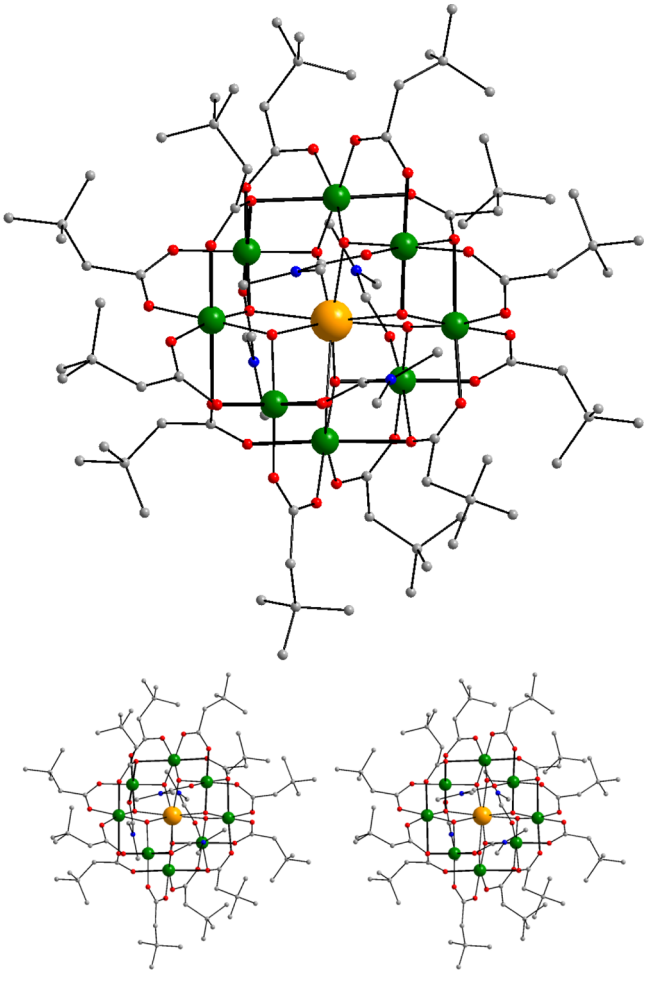

Figure 3. Structure and a stereopair of complex **2**. Thicker bonds denote Mn^{III} Jahn−Teller axes. Color code: Mn^{III} green, Ce^{IV} orange, N blue, O red, C gray. H atoms are omitted for clarity.

dx.doi.org/10.1021/ic500617f | Inorg. Chem. 2014, 53, 6805−6816

$[CeMn_8O_8]$ core is shown in Figure 4. Selected interatomic distances and angles are listed in Table 5. Complex **2** contains a

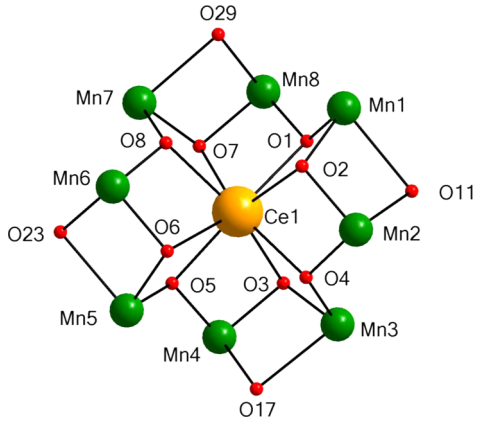

Figure 4. Labeled core of **2**, including the four monoatomically bridging carboxylate O atoms. Color code: Mn^{III} green, Ce^{IV} orange, O red, C gray.

$[CeMn_8O_8]^{12+}$ core consisting of a Ce^{IV} held within a nonplanar, saddlelike loop of eight Mn^{III} atoms by eight μ_3-O^{2-} ions. The metal oxidation states and the deprotonated nature of oxide ions were confirmed by BVS calculations (Tables 3 and 4). Mn atoms Mn2, Mn4, Mn6, and Mn8 occupy the corners of an almost perfect tetrahedron with Ce at the center (Mn−Ce−Mn angles = 108.6−109.9°), whereas the other four Mn atoms, namely, Mn1, Mn3, Mn5, and Mn7, form a distorted (flattened) tetrahedron (Mn−Ce−Mn angles = 90.7−93.8° and >158°). Peripheral ligation is provided by eight $\eta^1{:}\eta^1{:}\mu$- and four $\eta^1{:}\eta^2{:}\mu_3$-^{t}BuCH$_2$CO$_2^-$ groups, and a terminal DMF on each Mn. The Ce atom is eight-coordinate with distorted dodecahedral geometry, and the Ce−O lengths (2.31−2.40 Å) are typical for eight-coordination Ce^{IV}.[26] The Mn^{III} atoms are near-octahedral and display JT elongation axes, with the JT bonds being the four O(DMF)−Mn−O(carb) and four O(carb)−Mn−O(carb) axes (carb = carboxylate) at Mn(2,4,6,8) and Mn(1,3,5,7), respectively; that is, the JT axes all avoid the μ_3-O^{2-} ions.

Table 5. Selected Interatomic Distances (Å) for Complex 2

Mn1···Mn2	3.041(1)	Mn3−O12	2.165(2)
Mn1···Mn8	3.229(1)	Mn3−O17	2.303(2)
Mn2···Mn3	3.238(1)	Mn4−O3	1.879(2)
Mn5···Mn6	3.013(1)	Mn4−O5	1.857(2)
Mn7···Mn8	3.008(1)	Mn4−O16	1.983(2)
Mn1···Ce1	3.330(1)	Mn4−O19	1.981(2)
Mn3···Ce1	3.338(1)	Mn4−O17	2.289(2)
Mn5···Ce1	3.323(1)	Mn4−O35	2.221(2)
Mn7···Ce1	3.321(1)	Mn5−O5	1.875(2)
Ce1−O1	2.336(2)	Mn5−O6	1.876(2)
Ce1−O2	2.399(2)	Mn5−O20	1.966(2)
Ce1−O3	2.399(2)	Mn5−O21	1.976(2)
Ce1−O4	2.320(2)	Mn5−O18	2.147(2)
Ce1−O5	2.314(2)	Mn5−O23	2.308(2)
Ce1−O6	2.388(2)	Mn6−O6	1.876(2)
Ce1−O7	2.389(2)	Mn6−O8	1.857(2)
Ce1−O8	2.316(2)	Mn6−O22	1.986(2)
Mn1−O1	1.865(2)	Mn6−O25	1.983(2)
Mn1−O2	1.867(2)	Mn6−O23	2.298(2)
Mn1−O9	1.969(2)	Mn6−O34	2.206(2)
Mn1−O32	1.964(2)	Mn7−O7	1.876(2)
Mn1−O11	2.371(2)	Mn7−O8	1.869(2)
Mn1−O30	2.183(2)	Mn7−O26	1.969(2)
Mn2−O2	1.883(2)	Mn7−O27	1.973(2)
Mn2−O4	1.858(2)	Mn7−O24	2.143(2)
Mn2−O10	1.993(2)	Mn7−O29	2.321(2)
Mn2−O13	1.973(2)	Mn8−O1	1.857(2)
Mn2−O11	2.240(2)	Mn8−O7	1.878(2)
Mn2−O33	2.215(2)	Mn8−O28	1.984(2)
Mn3−O3	1.881(2)	Mn8−O31	1.988(2)
Mn3−O4	1.856(2)	Mn8−O29	2.247(2)
Mn3−O14	1.972(2)	Mn8−O36	2.225(2)
Mn3−O15	1.978(2)		

Complex **2** joins a growing family of $[CeMn_8O_{12}(O_2CR)_{12}(solv)_4]$ complexes with the saddlelike topology, differing in the carboxylate identity and/or terminal solvent molecules (solv).[8c,26,27] Although structurally similar, these complexes have differing magnetic properties, and in this regard **2** is different from all previous members (vide infra). In anticipation of the magnetic discussion below, we compare in Table 6 the core structural parameters pertinent to the pairwise Mn_2 exchange interactions, namely, M···M distances and M−O−M angles. The complexes are all remarkably similar with respect to the metric parameters within the $[CeMn_8O_8]^{12+}$ core, which are essentially all indistinguishable by the usual 3σ statistical criterion. The main statistically significant exception to this is found in the Mn−OR−Mn angles (RO^- = monoatomically bridging carboxylate O atom), where those for the second and fifth entries in the table are ∼2° greater than the others. This could be of relevance to the magnetic properties, because this O atom lies on the JT axes of both the Mn atoms it bridges (vide supra) and thus represents the superexchange pathway for interaction of their two d_{z^2} magnetic orbitals. The exchange interaction between these two Mn atoms should thus be sensitive to the Mn−OR−Mn angle, since small changes to such acute bridging angles can often have significant effects on the exchange coupling (vide infra).

A PovRay representation of $[Ce_2Mn_4O_2(O_2CMe)_6(NO_3)_4(hmp)_4]$ (**3**) and a stereopair are presented in Figure 5, and its labeled core is shown in Figure 6. Selected interatomic distances and angles are listed in Table 7. Complex **3** is similar to **1** in containing an M_6 octahedron, but it is now a heterometallic $[Ce_2Mn_4O_2]$ octahedral core consisting of two Ce^{III} and four Mn^{III} atoms bridged by two μ_4-O^{2-} ions. The metal oxidation states were established by BVS calculations (Table 3). The core is additionally held together by four μ-RO^- alkoxide arms of the $\eta^2{:}\eta^1{:}\mu$-hmp$^-$ groups, and two $MeCO_2^-$ ligands in a very rare $\eta^2{:}\eta^2{:}\mu_3$ bridging mode between two Mn^{III} and one Ce^{III}. Peripheral ligation is completed by four $\eta^1{:}\eta^1{:}\mu$ acetates bridging $Mn^{III}{}_2$ pairs and by two chelating nitrate groups on each Ce. The Mn^{III} atoms exhibit clear JT axial elongations along the O(carb)−Mn−O(carb) axes, which again avoid the bridging O^{2-} ions, as expected. As a result of the asymmetric positions of the different core bridging ligands, the octahedron is very distorted, with the Mn_4 equatorial plane being a rhombus rather than a square (Mn1···Mn2 = 3.198(1), Mn1···Mn2′ = 5.115(1) Å). The Ce atoms are located 2.026 Å above and below this plane (Supporting Information, Figure S2). Another Ce_2Mn_4 cluster with a similar core but with different carboxylates and chelate is known,[27] but a third reported example is at the $Ce^{III}{}_2Mn^{IV}{}_4$ oxidation level and has a very different structure from **3**.[31]

dx.doi.org/10.1021/ic500617f | Inorg. Chem. 2014, 53, 6805−6816

Table 6. Magnetostructural Correlation for 2 and Other $[CeMn_8O_{12}(O_2CR)_{12}(solv)_4]$ Clusters

R	$CH_2{}^tBu$	Me	Me	Ph	HPh_2	^tBu
solv	DMF (**2**)	H_2O	py	MeCN	H_2O	DMF
space group	$P\bar{1}$	$I\bar{4}$	$P4_2/n$	$P4n2$	$P2_1/n$	$P\bar{1}$
Mn···Mn	3.025(15)[a]	3.029(7)	3.034(1)	3.011(1)	3.04(1)[a]	3.018(18)[a]
	3.235(5)[a]	3.240(8)	3.237(1)	3.255(1)	3.21(1)[a]	3.245(7)[a]
Ce···Mn	3.345(25)[a]	3.345(5)	3.331(1)	3.309(1)	3.36(1)[a]	3.346(29)[a]
		3.356(5)	3.348(1)	3.320(1)		
Mn−OR−Mn	82.1(4)[a]	84.5(1)	82.4(1)	81.5(1)	84.2(1.3)[a]	82.2(5)
$Mn-O^{2-}-Mn$	121.0(1.3)[a]	122(1)	121.4(2)	123.3(2)	119.8(6)[a]	121.8(1.1)[a]
	107.1(1.2)[a]	106(1)	106.8(2)	107.0(2)	102.3(2.6)[a]	106.9(7)[a]
Mn−O−Ce	102.7(1.1)[a]	102.9(1.1)[a]	102.35(35)[a]	101.4(1)[a]	102.45(65)[a]	102.32(91)[a]
	105.5(1.2)[a]	105.85(5)[a]	105.95(65)[a]	105.25(35)[a]	106.0(9)[a]	105.7(1.4)[a]
S	0	16	4 or 5	n.r.	6 ± 1	5
SMM[b]	no	yes[c]	no	n.r.	yes[d]	no
ref.	t.w.	8c, 26b	26b	26b	26b	27

[a]Average value; number in parentheses is the ± range of individual values about the mean. [b]SMM = single-molecule magnet. [c]SMM with weak exchange-bias due to H-bonded one-dimensional chain formation. [d]SMM with fast tunneling at zero field; n.r. = not reported; t.w. = this work.

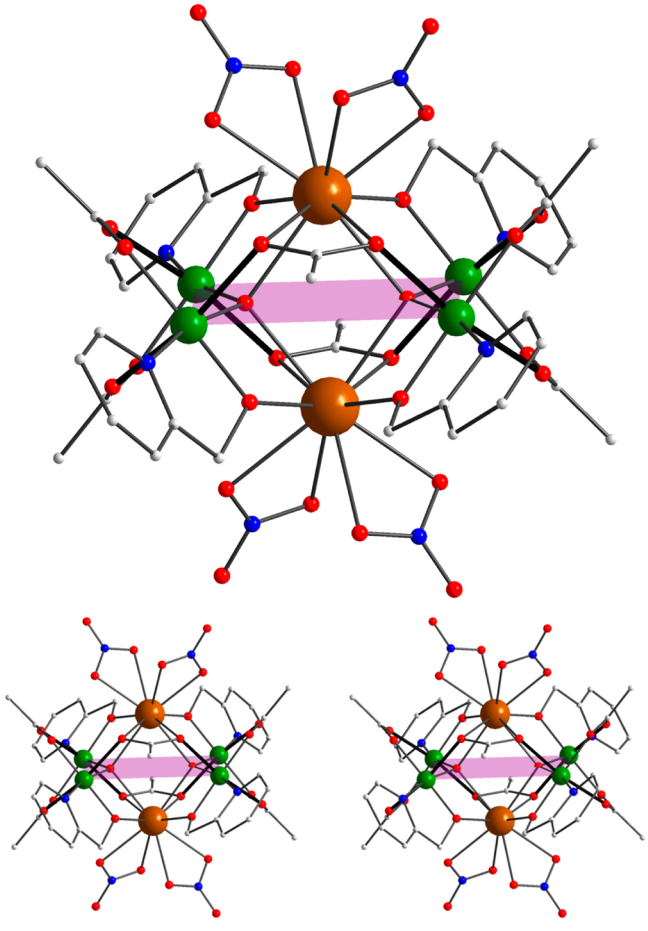

Figure 5. Structure and a stereopair of complex **3**. Thicker bonds denote Jahn−Teller elongation axes. Color code: Mn^{III} green, Ce^{III} brown, N blue, O red, C gray. H atoms are omitted for clarity.

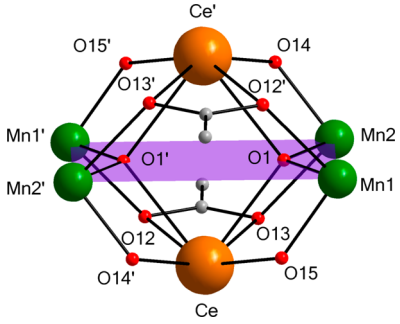

Figure 6. Labeled core of **3**, including the $\eta^2{:}\eta^2{:}\mu_3$-acetate ligands and other monoatomically bridging acetate O atoms; primed and unprimed atoms are related by the inversion center. Color code: Mn^{III} green, Ce^{III} brown, O red, C gray. H atoms are omitted for clarity.

Table 7. Selected Interatomic Distances (Å) and Angles (deg) for Complex 3

Ce···Mn1	3.742(1)	Ce−O12	2.716(2)
Ce···Mn2	3.534(1)	Mn1−O8	1.927(2)
Mn1···Mn2	3.198(1)	Mn1−N3	2.039(3)
Mn1···Mn2′	5.115(1)	Mn1−O10	2.160(2)
Ce−O14′	2.470(2)	Mn1−O12′	2.274(2)
Ce−O15	2.153(8)	Mn2−O1	1.887(2)
Ce−O1	2.557(2)	Mn2−O14	1.888(2)
Ce−O2	2.561(3)	Mn2−O11	1.927(2)
Ce−O1′	2.563(2)	Mn2−N4	2.005(7)
Ce−O6	2.566(2)	Mn2−O9	2.157(3)
Ce−O5	2.619(2)	Mn2−O13	2.329(2)
Ce−O3	2.628(3)	Mn1−O15	1.879(2)
Ce−O13	2.638(2)	Mn1−O1	1.893(2)
Ce−O1−Ce′	105.45(7)	Mn2−O1−Mn1	115.62(10)
Mn1′−O12−Ce	96.73(8)	Mn2−O1−Ce	113.12(9)
Mn2−O13−Ce	97.02(8)	Mn1−O1−Ce	104.94(8)
Mn2−O14−Ce′	107.61(9)	Mn2−O1−Ce′	104.10(8)
Mn1−O15−Ce	107.63(9)	Mn1−O1−Ce′	113.35(9)

Complexes **1**, **2**, and **3** join a growing family of Mn/Ce clusters. We listed selected Mn/Ce clusters in Table 8 for a convenient comparison of their structural types and pertinent magnetic data such as their ground-state spin (*S*) values (vide infra). The core of **1** is unprecedented.

Magnetochemistry. DC Magnetic Susceptibility Studies. Solid-state, variable-temperature magnetic susceptibility measurements were performed on dried microcrystalline samples of $1{\cdot}4H_2O$, **2**, and $3{\cdot}2H_2O$. DC susceptibility (χ_M) data on samples suspended in eicosane to prevent torquing

dx.doi.org/10.1021/ic500617f | Inorg. Chem. 2014, 53, 6805−6816

Table 8. Formulas, Core Types, and Ground-State Spin for Selected Ce/Mn Clusters

complex	core	Ce/Mn ratio	S	ref.
$[CeMn_2O_3(O_2CMe)(NO_3)_4(H_2O)_2(bpy)_2]^{+a}$	$[Ce^{IV}Mn^{IV}_2(\mu\text{-}O)_3]$	0.5	0	8a, 8b
$[Ce_3Mn_2O_6(O_2CMe)_6(NO_3)_2(mhpH)_4]^b$	$[Ce^{IV}_3Mn^{IV}_2(\mu_3\text{-}O)_6]$	1.5	0	8a, 8b
$[Ce_3Mn_2O_6(O_2CMe)_6(NO_3)_2(pyroH)_2(H_2O)_3]^b$	$[Ce^{IV}_3Mn^{IV}_2(\mu_3\text{-}O)_6]$	1.5	0	8a, 8b
$[Ce_2Mn_4O_2(O_2CMe)_6(NO_3)_4(hmp)_4]^c$	$[Ce^{III}_2Mn^{III}_4(\mu_4\text{-}O)_2]$	0.5	0^d	t.w.
$[Ce_2Mn_4O_2(^tBuCO_2)_6(pic)_2(H_2O)_2$	$[Ce^{III}_2Mn^{III}_4(\mu_4\text{-}O)_2]$	0.5	0	27
$[Ce_2Mn_4O_2(Me\text{-}sao)_6(NO_3)_4(OAc)_2(H_2O)_2]^e$	$[Ce^{III}_2Mn^{IV}_4\ (\mu_3\text{-}O)_2]$	0.5	3/2	31
$[CeMn_6O_9(O_2CMe)_9(NO_3)(H_2O)_2]^f$	$[Ce^{IV}Mn^{IV}_6(\mu_3\text{-}O)_6(\mu\text{-}O)_3]$	0.17	0	8
$[CeMn_6O_9(O_2CMe)_9(MeOH)(H_2O)_2]^{+f}$	$[Ce^{IV}Mn^{IV}_6(\mu_3\text{-}O)_6(\mu\text{-}O)_3]$	0.17	0	8
$[CeMn_8O_8(O_2CMe)_{12}(H_2O)_4]^g$	$[Ce^{IV}Mn^{III}_8(\mu_3\text{-}O)_8]$	0.125	16	8c, 26
$[CeMn_8O_8(O_2CMe)_{12}(py)_4]^g$	$[Ce^{IV}Mn^{III}_8(\mu_3\text{-}O)_8]$	0.125	4 or 5	26
$[CeMn_8O_8(O_2CPh)_{12}(solv)_4]^g$	$[Ce^{IV}Mn^{III}_8(\mu_3\text{-}O)_8]$	0.125	n.r.	26
$[CeMn_8O_8(O_2CCHPh_2)_{12}(H_2O)_4]^g$	$[Ce^{IV}Mn^{III}_8(\mu_3\text{-}O)_8]$	0.125	6 ± 1	26
$[CeMn_8O_8(O_2CCH_2{}^tBu)_{12}(DMF)_{14}]^g$	$[Ce^{IV}Mn^{III}_8(\mu_3\text{-}O)_8]$	0.125	0	t.w.
$[Ce_6Mn_4O_{12}(O_2CMe)_{10}(NO_3)_4(py)_4]^h$	$[Ce^{IV}_6Mn^{III}_2Mn^{IV}_2(\mu_3\text{-}O)_8(\mu_4\text{-}O)_4]$	1.5	1	t.w.
$[Ce_4Mn_{10}O_{10}(OMe)_6(O_2CPh)_{16}(NO_3)_2(solv)_4]^i$	$[Ce^{IV}_2Ce^{III}_2Mn^{III}_{10}(\mu_3\text{-}O)_4(\mu_4\text{-}O)_6]$	0.4	4	6c

[a] $[Mn^{IV}_2O_2]$ rhomb linked to Ce^{IV} via a linear O^{2-}. [b] Ce^{IV}_3 triangle with Mn^{IV} at the apexes of a trigonal bipyramid. [c] Mn^{III}_4 parallelogram with Ce^{III} at the apexes of a highly distorted octahedron. [d] The spin of the Mn_4 unit. Abbreviations: bpy = 2,2′-bipyridine, mhpH = 6-methyl-2-hydroxypyridine, pyro = 2-pyrrolidinone, Me-saoH$_2$ = methyl salicylaldoxime, t.w. = this work, n.r. = not reported. [e] Two $[Mn^{IV}_2Ce^{III}O]$ triangles linked by oximato groups. [f] Ce^{IV} held within a Mn^{IV}_6 wheel by six O^{2-} ions. [g] Ce^{IV} held within a saddlelike Mn^{III}_8 loop by eight O^{2-} ions. [h] Central $Ce^{IV}_6O_8$ octahedron face-fused to two $[Mn^{III/IV}_2Ce^{IV}_2O_4]$ cubanes. [i] solv = MeOH, H_2O; central $[Mn^{III}_4Ce^{IV}_2O_6(OMe)_2]$ unit fused at either end to $[Mn^{III}_3Ce^{III}O_2(OMe)_2]$ cubane.

were collected in the 5.0−300 K range in a 0.1 T (1000 G) magnetic field.

The data for **1**·4H$_2$O are plotted as $\chi_M T$ versus T in Figure 7. The $\chi_M T$ value is 3.58 cm^3 K mol^{-1} at 300 K and steeply decreases with decreasing temperature to 0.69 cm^3 K mol^{-1} at 5.0 K. Since Ce^{IV} is diamagnetic, the data indicate strongly antiferromagnetic (AF) interactions within each $Mn^{III}Mn^{IV}$ unit. The data were fit to a model that assumes each molecule of **1** to contain two independent $Mn^{III}Mn^{IV}$ dinuclear units; long-range interactions between Mn_2 units through the central Ce_6 octahedron are expected to be essentially zero and likely weaker than interactions between two Mn_2 of different molecules through the π-stacking interactions. The isotropic Heisenberg spin Hamiltonian describing an exchange-coupled $Mn^{III}Mn^{IV}$ unit is given by eq 4, and the energy $E(S)$ of each resultant S of the molecule is given by the eigenvalue eq 5, where J is the exchange coupling parameter between the two Mn ions, S_1 = 2, and S_2 = $^3/_2$.

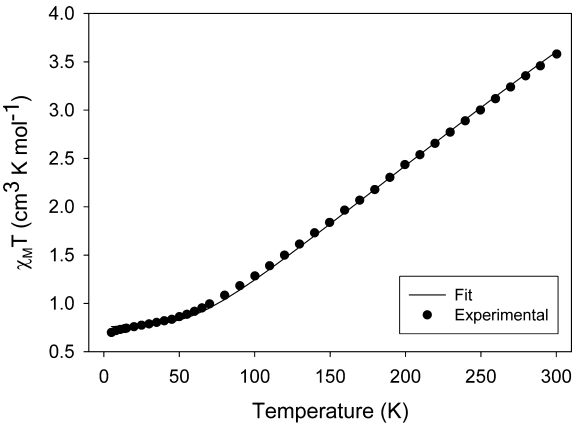

Figure 7. $\chi_M T$ vs T plot for **1**·4H$_2$O in a 1000 G DC field. The solid line is the fit of the data to the theoretical equation; see the text for the fit parameters.

$$\mathcal{H} = -2J\hat{S}_1\cdot\hat{S}_2 \tag{4}$$

$$E(S) = -J[S(S+1)] \tag{5}$$

The $\chi_M T$ versus T data were fit to the theoretical equation for such a system derived from the Van Vleck equation,[32] and the obtained fit (solid line in Figure 7) had parameters J = −60.4(7) cm^{-1} and g = 2.00(1). This indicates an S = 1/2 ground state well-isolated from an S = $^3/_2$ first excited ground

Table 9. Magnetostructural Comparison of the $[Mn^{III}(O^{2-})_2Mn^{IV}]$ Unit in 1 with those in Dinuclear Complexes

complex	M···M (Å)	M−O−M (deg)	M−O (Å)	J (cm^{-1})	ref.
$[Mn_2O_2(bpy)_4]^{3+}$	2.716	95.6	1.819	−150	39
$[Mn_2O_2(phen)_4]^{3+}$	2.711	96.9	1.812	−134	40
$[Mn_2O_2(tren)_2]^{3+}$	2.679	95.35	1.812	−146	41
$[Mn_2O_2(bispicMe_2en)_2]^{3+}$	2.679	94.6	1.822	−160	42
$[Mn_2O_2(bispicMe_2en(chxn))_2]^{3+}$	2.699	93.8	1.849	−147	42
$[Mn_2O_2(bisimMe_2en)_2]^{3+}$	2.677	94.6	1.821	−136	43
$[Mn_2O_2(bispicen)_2]^{3+}$	2.672	95.0	1.811	−140	44
$[Mn_2O_2(L_3)_2]^{3+}$	2.693	96.0	1.812	−177	45
$[Mn_2O_2(L_4)_2]^{3+}$	2.682	95.6	1.810	−221	45
$[Mn_2(N_3O\text{-}py)_2(O)_2]^{3+}$	2.656	94.6	1.810	−151	46
1	2.809	97.8	1.864	−60	this work

dx.doi.org/10.1021/ic500617f | Inorg. Chem. 2014, 53, 6805−6816

state at 181(2) cm^{-1} higher in energy. The $\chi_M T$ value at the lowest temperatures is thus consistent with two separate $S = 1/2$ units per molecule of **1** (expected 0.75 cm^3 K mol^{-1} if $g = 2.0$).

The obtained J value for **1** is weaker than those for $[Mn^{III}(\mu_2\text{-}O^{2-})_2Mn^{IV}]$ dinuclear units, which typically have $J = -100$ to -220 cm^{-1}.[33,34] This can be attributed to the oxide ions being μ_3 by linking to the strongly Lewis-acidic Ce^{4+} ions, as reflected in slightly increased Mn···Mn distances, Mn−O^{2-} bond lengths, and Mn−O^{2-}−Mn angles. These structural parameters and J values for **1** and dinuclear $[Mn^{III}(\mu_2\text{-}O^{2-})_2Mn^{IV}]$ complexes are compared in Table 9. The same effect was seen and discussed in detail for bis-oxide-bridged $Mn^{IV}Mn^{IV}$ pairs bound to Ce^{4+} ions.[8b]

The $\chi_M T$ versus T data for **2** and **3**·2H_2O are shown in Figure 8. For **2**, the $\chi_M T$ value increases from 26.01 cm^3 K mol^{-1} at 300 K to a maximum of 30.10 cm^3 K mol^{-1} at 90 K, then drops rapidly to 4.72 cm^3 K mol^{-1} at 5.0 K, and appears to be heading for zero at 0 K. The $\chi_M T$ value at 300 K is slightly greater than the spin-only ($g = 2.0$) value for eight noninteracting Mn^{III} ions of 24.00 cm^3 K mol^{-1}, so the plot suggests a combination of weak ferro- and antiferromagnetic interactions are present within **2**. Given the high nuclearity and low symmetry of the complex, and the expected weak couplings and low-lying excited states suggested by Figure 8, we resorted to AC susceptibility measurements to determine the ground state of the molecule (vide infra).

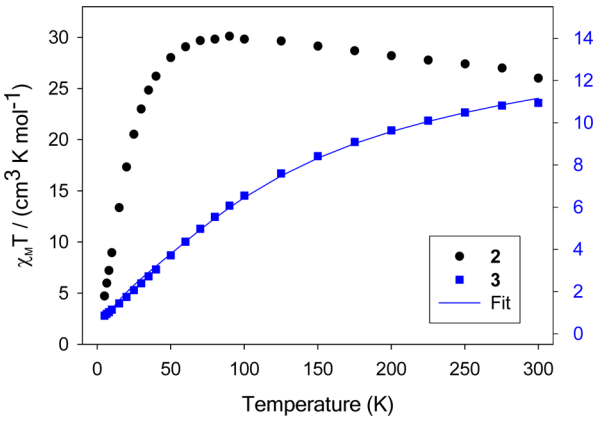

Figure 8. $\chi_M T$ vs T plots for **2** and **3**·2H_2O in a 1000 G DC field.

For **3**·2H_2O, the $\chi_M T$ value decreases from 10.90 cm^3 K mol^{-1} at 300 K to 7.61 cm^3 K mol^{-1} at 130 K, and then drops rapidly to 0.92 cm^3 K mol^{-1} at 5 K (Figure 8). The $\chi_M T$ value at 300 K, 10.90, is slightly lower than expected for four Mn^{III} and two Ce^{III} ($S = 1/2$, $L = 3$, $^2F_{5/2}$ free-ion, $\chi_M T = 0.81$ cm^3 K mol^{-1})[35] noninteracting ions (13.6 cm^3 K mol^{-1}), indicating the presence of dominant AF interactions. The plot appears to be heading for a small but nonzero value at 0 K, suggesting the Mn_4 unit is in a diamagnetic ground state with some paramagnetism remaining from weakly coupled Ce^{III} atoms. This was confirmed by the AC studies below 15 K (vide infra), which show a near temperature-independent $\chi'_M T$. Therefore, the decrease in $\chi_M T$ in the 20−300 K range is due to AF interactions within the central Mn_4 unit. In fact, the structure of the core (Figure 6) suggests that, magnetically, **3** can be considered to a first approximation as two $[Mn^{III}_2(\mu\text{-}O^{2-})(\mu\text{-}RCO_2^-)_2]$ units, because the interactions between them, and between them and the Ce atoms, should both be very weak. Thus, we fit the data to the Van Vleck equation derived by assuming the isotropic spin Hamiltonian of eq 4 with $S_1 = S_2 = 2$. A good fit was obtained with $J = -9.0(5)$ cm^{-1} and $g = 2.00(1)$ (solid line in Figure 8). Such a weak AF J value is as expected for the $[Mn^{III}_2(\mu\text{-}O^{2-})(\mu\text{-}RCO_2^-)_2]$ unit.[33b,36]

AC Magnetic Susceptibility Studies. To further probe the ground states of **1**·4H_2O, **2**, and **3**·2H_2O, AC susceptibility data were collected in the 1.8−15 K temperature range in a 3.5 G field oscillating at 50−1000 Hz frequencies. The in-phase AC susceptibility (χ'_M) is shown as $\chi'_M T$ versus T in Figure 9. For

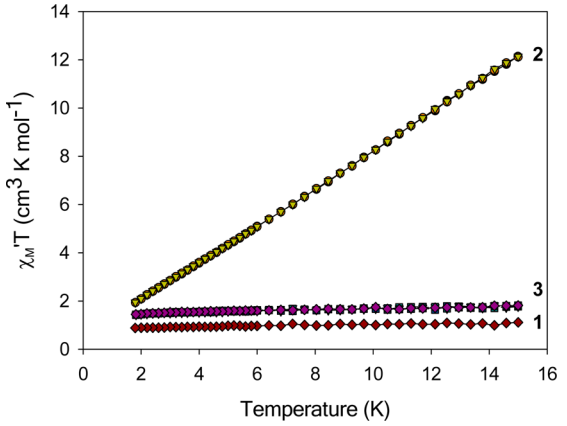

Figure 9. $\chi'_M T$ vs T plots (χ'_M is the in-phase AC susceptibility) signals, for **1**·4H_2O, **2**, and **3**·2H_2O at 500 Hz (●) and 250 Hz (▲).

1·4H_2O, $\chi'_M T$ is essentially constant in this temperature range and extrapolates to ∼0.7 cm^3 K mol^{-1} at 0 K. This is consistent with the DC data and its interpretation that **1** behaves as two noninteracting $S = 1/2$ Mn_2 units (total 0.75 cm^3 K mol^{-1} if $g = 2.0$). There was no out-of-phase χ'' susceptibility signal (Supporting Information, Figure S3).[30] For **2**, $\chi'_M T$ decreases steeply with decreasing temperature from ∼12.1 cm^3 K mol^{-1} at 15 K to 1.86 cm^3 K mol^{-1} at 1.8 K. This rapid decrease is consistent with depopulation of very low-lying excited states. Extrapolation of the data indicates $\chi'_M T$ to be heading for zero at 0 K, indicating an $S = 0$ ground state. This is the first time this ground state has been obtained for a member of this $[Ce^{IV}Mn^{III}_8O_{12}(O_2CR)_{12}(solv)_4]$ family, and means that both the lowest ($S = 0$) and highest ($S = 16$) ground states have now been attained, with R/solv of $O_2CCH_2{}^tBu$/DMF and Me/H_2O, respectively, as well as various intermediate S ground states for other members of the family (Table 8). Such a range of ground states, from the minimum to the maximum, in such a high nuclearity cluster with a given structure is unprecedented. The first two entries in Table 6 are the $S = 0$ and 16 complexes, and their structural parameters are essentially identical within statistical uncertainties, except for the Mn−OR−Mn angles, as stated earlier. It would be inappropriate to correlate the ground state with this one parameter, however, since the fifth entry also has a larger angle comparable with the second, and yet its ground state is $S \approx 6$, not 16. The safest conclusion to be drawn, especially since these complexes have low-lying excited states, is that the ground-state differences are not due to any one parameter but are the result of many small structural variations and their resulting perturbation of all the exchange interactions in the molecule.

For **3**·2H_2O, $\chi'_M T$ is essentially constant below 15 K, decreasing only slightly from 1.5 cm^3 K mol^{-1} at 15 K to 0.7 cm^3 K mol^{-1} at 1.8 K, extrapolating to ∼0.6 cm^3 K mol^{-1} at 0

dx.doi.org/10.1021/ic500617f | Inorg. Chem. 2014, 53, 6805−6816

K. We interpret this behavior to indicate a predominantly AF system with the slight paramagnetism remaining at the lowest temperatures resulting from the weakly coupled Ce^{III} atoms. There were no out-of-phase χ'' signals (Supporting Information, Figure S5).[30]

Electron Paramagnetic Resonance Studies. EPR studies were carried out on frozen solutions of **1** in a 1:1 mixture of MeCN/pyridine, and the spectrum at 20 K is shown in Figure 10. The spectrum exhibits the typical ~16-line hyperfine

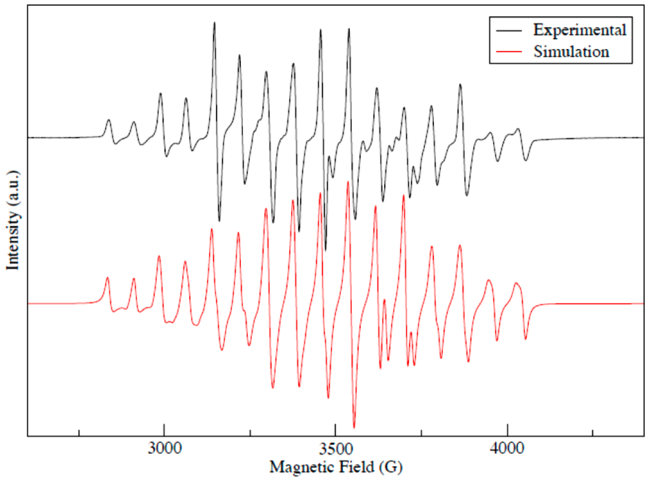

Figure 10. EPR spectrum of **1** in a 1:1 mixture of MeCN/pyridine at 20 K (top) and the simulated spectrum (bottom); see the text for the simulation parameters.

splitting (^{55} Mn, $I = {}^5/_2$, 100%) displayed by dinuclear complexes containing the $[Mn^{III}(\mu\text{-}O^{2-})_2Mn^{IV}]$ unit arising from a near $A(Mn^{3+}) = 2A(Mn^{4+})$ relationship of the two hyperfine coupling constants (A). Additional features and splittings are assignable to anisotropy in g and A. The line widths of the individual hyperfine features range from 80 to 120 mT. The spectrum was simulated to obtain the components of the g and A tensors using the program EasySpin.[37] The simulation shown in Figure 10 was obtained assuming axial symmetry in g and A, and inclusion of a second-order perturbation: the simulation parameters were $g_{\|} = 1.961$, $g_{\perp} = 1.953$, $A_{1\perp} = 446$ MHz, $A_{1\|} = 410$ MHz, $A_{2\perp} = 220$ MHz, and $A_{2\|} = 210$ MHz; the simulation without second-order effects is only a little different (Supporting Information, Figure S6).[30] Attempts to simulate the spectrum assuming rhombic symmetry led to inferior agreement with the experimental spectrum (Supporting Information, Figure S7).

The simulation parameters obtained for **1** are compared with those for dinuclear $[Mn_2(\mu\text{-}O^{2-})_2]^{3+}$ complexes in Table 10, where it can be seen that they are quite similar; the slight differences for **1** can be assigned to the different environment of its Mn_2 unit within a Ce_6Mn_4 cluster. Un and co-workers[38] have reported a linear correlation between the Δg, the difference between $g_{\perp}$ and $g_{\|}$, and the average Mn−N bond lengths in dinuclear $[Mn_2(\mu\text{-}O^{2-})_2]^{3+}$ complexes. Although **1** has only two N-based ligands at each Mn_2 unit, we find its Δg and Mn−N distances to agree with the reported correlation; as shown in Figure 11, including the data for **1** gives a linear correlation with $R^2 = 0.997$.

Table 10. Effective Spin Parameters Determined from Simulation of EPR Spectra[a]

complex	$g_{\perp}$	$g_{\|}$	$A_{1\perp}$	$A_{1\|}$	$A_{2\perp}$	$A_{2\|}$
bisimMe	1.999	1.982	460	337	217	230
bispicenMe	2.006	1.988	458	351	215	223
bisimH2	1.998	1.981	464	362	218	223
bipy	1.997	1.981	487	345	210.5	229
phen	1.998	1.981	482	339	211	233
1	1.961	1.953	446	410	220	210

[a]Hyperfine couplings are in MHz. This table is adapted from that previously reported by Un and co-workers.[38]

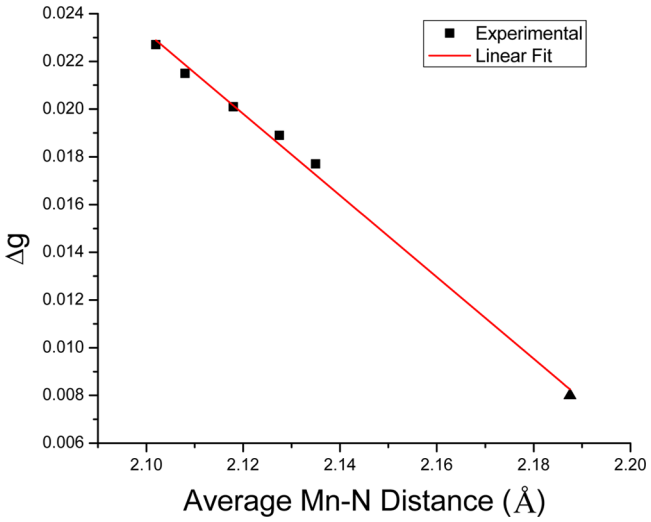

Figure 11. Plot of Δg ($= g_{\perp} - g_{\|}$) vs the average Mn−N distance (Å) for selected dinuclear complexes containing the $[Mn^{III}/Mn^{IV}O_2]$ core. ■ = data taken from ref 38; ▲ = complex **1**.

■ CONCLUSIONS

Three new Ce/Mn clusters are reported in this work, two of which are new structural types in this area, and all three of which are noteworthy in one way or another. The structures of **1** and **3** are fascinating and, in fact, somewhat related in that they can both be described as Mn_2 units connected by a Ce_x unit. In contrast, **2** is a new member of a well-known structural type, but it is nevertheless highly interesting in that it has an $S = 0$ ground state, the first for this family. As stated above, both the minimum $S = 0$ and maximum $S = 16$ ground states have now been obtained for these $Mn^{III}{}_8Ce^{IV}$ clusters, and it serves to emphasize how small structural perturbations within a system with many competing exchange interactions of comparable magnitude can have major and unpredictable effect on the identity of the ground-state spin. In the present case, variation of the carboxylate R group, from small acetate to bulky diphenylacetate and now *tert*-butyl acetate in **2**, has been the cause, as well as the identity of terminal bound solvent molecules. The core structures are almost superimposable, however, and it is remarkable how such subtle structural changes can have such massive magnetic consequences. Finally, the area of Ce/Mn chemistry clearly continues to produce noteworthy results, and further results in this area will be reported in due course.

dx.doi.org/10.1021/ic500617f | Inorg. Chem. 2014, 53, 6805−6816

■ ASSOCIATED CONTENT

Supporting Information

X-ray crystallographic data in CIF format for complexes **1**·2py·6MeCN, **2**·$^3/_2$DMF, and **3**·H_2O·6MeCN; molecular packing in **1**·2py·6MeCN; out-of-phase AC magnetic susceptibility data for **1**·$4H_2O$, **2**, and **3**·$2H_2O$, and EPR simulations for **1**. This material is available free of charge via the Internet at http://pubs.acs.org.

■ AUTHOR INFORMATION

Corresponding Author

*E-mail: christou@chem.ufl.edu. Phone: +1-352-392-8314. Fax: +1-352-392-8757.

Present Address

[†]Department of Chemistry, University of North Florida, Jacksonville, Florida 32224.

Notes

The authors declare no competing financial interest.

■ ACKNOWLEDGMENTS

We thank the National Science Foundation (Grant No. DMR-1213030) for support of this work, and Umar Twahir and Prof. Alex Angerhofer for help collecting the EPR data.

■ REFERENCES

(1) (a) Sessoli, R.; Tsai, H. L.; Schake, A. R.; Wang, S.; Vincent, J. B.; Folting, K.; Gatteschi, D.; Christou, G.; Hendrickson, D. N. *J. Am. Chem. Soc.* **1993**, *115*, 1804−1816. (b) Christou, G.; Gatteschi, D.; Hendrickson, D. N.; Sessoli, R. *MRS Bull.* **2000**, *25*, 66−71. (c) Christou, G. *Polyhedron* **2005**, *24*, 2065−2075. (d) Sessoli; Gatteschi, D.; Caneschi, A.; Novak, M. A. *Nature* **1993**, *365*, 141−143. (e) Wernsdorfer, W.; Aliaga-Alcalde, N.; Hendrickson David, N.; Christou, G. *Nature* **2002**, *416*, 406−409.

(2) Friedman, J. R.; Sarachik, M. P.; Tejada, J.; Ziolo, R. *Phys. Rev. Lett.* **1996**, *76*, 3830−3833.

(3) (a) Wernsdorfer, W.; Sessoli, R. *Science* **1999**, *284*, 133−135. (b) Wernsdorfer, W.; Soler, M.; Christou, G.; Hendrickson, D. N. *J. Appl. Phys.* **2002**, *91*, 7164−7167. (c) Wernsdorfer, W.; Chakov, N. E.; Christou, G. *Phys. Rev. Lett.* **2005**, *95*, 037203(1−4).

(4) (a) Prasad, T. K.; Rajasekharan, M. V.; Costes, J.-P. *Angew. Chem., Int. Ed.* **2007**, *46*, 2851−2854. (b) Zaleski, C. M.; Kampf, J. W.; Mallah, T.; Kirk, M. L.; Pecoraro, V. L. *Inorg. Chem.* **2007**, *46*, 1954−1956. (c) Karotsis, G.; Kennedy, S.; Teat, S. J.; Beavers, C. M.; Fowler, D. A.; Morales, J. J.; Evangelisti, M.; Dalgarno, S. J.; Brechin, E. K. *J. Am. Chem. Soc.* **2009**, *132*, 12983−12990.

(5) (a) Liu, F. C.; Zeng, Y. F.; Jiao, J.; Li, J. R.; Bu, X. H.; Ribas, J.; Batten, S. R. *Inorg. Chem.* **2006**, *45*, 6129−6131. (b) Murugesu, M.; Mishra, A.; Wernsdorfer, W.; Abboud, K. A.; Christou, G. *Polyhedron* **2006**, *25*, 613−625.

(6) (a) Mishra, A.; Wernsdorfer, W.; Parsons, S.; Christou, G.; Brechin, E. K. *Chem. Commun.* **2005**, *41*, 2086−2088. (b) Mishra, A.; Wernsdorfer, W.; Abboud, K. A.; Christou, G. *J. Am. Chem. Soc.* **2004**, *126*, 15648−15649. (c) Mishra, A.; Tasiopoulos, A. J.; Wernsdorfer, W.; Abboud, K. A.; Christou, G. *Inorg. Chem.* **2007**, *46*, 3105−3115.

(7) (a) Lampropoulos, C.; Stamatatos, T. C.; Abboud, K. A.; Christou, G. *Inorg. Chem.* **2009**, *48*, 429−431. (b) Stamatatos, T. C.; Teat, S. J.; Wernsdorfer, W.; Christou, G. *Angew. Chem., Int. Ed.* **2009**, *48*, 521−524.

(8) (a) Tasiopoulos, A. J.; O'Brien, T. A.; Abboud, K. A.; Christou, G. *Angew. Chem., Int. Ed.* **2004**, *43*, 345−349. (b) Tasiopoulos, A. J.; Milligan, P. L., Jr; Abboud, K. A.; O'Brien, T. A.; Christou, G. *Inorg. Chem.* **2007**, *46*, 9678−9691. (c) Tasiopoulos, A. J.; Wernsdorfer, W.; Moulton, B.; Zaworotko, M. J.; Christou, G. *J. Am. Chem. Soc.* **2003**, *125*, 15274−15275.

(9) (a) Oshio, H.; Nihei, M.; Koizumi, S.; Shiga, T.; Nojiri, H.; Nakano, M.; Shirakawa, N.; Akatsu, M. *J. Am. Chem. Soc.* **2005**, *127*, 4568−4569. (b) Mereacre, V.; Ako, A. M.; Clerac, R.; Wernsdorfer, W.; Filoti, G.; Bartolome, J.; Anson, C. E.; Powell, A. K. *J. Am. Chem. Soc.* **2007**, *129*, 9248−9249. (c) Mereacre, V.; Ako, A. M.; Clerac, R.; Wernsdorfer, W.; Hewitt, I. J.; Anson, C. E.; Powell, A. K. *Chem.—Eur. J.* **2008**, *14*, 3577−3584. (d) Langley, S.; Moubaraki, B.; Murray, K. S. *Dalton Trans.* **2010**, *39*, 5066−5069. (e) Timco, G. A.; Batsanov, A. S.; Larsen, F. K.; Muryn, C. A.; Overgaard, J.; Teat, S. J.; Winpenny, R. E. P. *Chem. Commun.* **2005**, *41*, 3649−3651.

(10) (a) Wernsdorfer, W.; Mailly, D.; Timco, G. A.; Winpenny, R. E. P. *Phys. Rev. B* **2005**, *72*, 060409(1−4). (b) Wang, W. G.; Zhou, A. J.; Zhang, W. X.; Tong, M. L.; Chen, X. M.; Nakano, M.; Beedle, C. C.; Hendrickson, D. N. *J. Am. Chem. Soc.* **2007**, *129*, 1014−1015.

(11) (a) Holyńska, M.; Premužić; Jeon, I.- R.; Wernsdorfer, W.; Clérac, R.; Dehnen, S. *Chem.—Eur. J.* **2011**, *17*, 9605−9610. (b) Liu, C.-M.; Zhang, D.-Q.; Zhu, D.-B. *Dalton Trans.* **2010**, *39*, 11325−11328.

(12) (a) Yagi, M.; Kaneko, M. *Chem. Rev.* **2001**, *101*, 21−36. (b) Ruettinger, W.; Dismukes, G. C. *Chem. Rev.* **1997**, *97*, 1−24. (c) Manchanda, R.; Brudvig, G. W.; Crabtree, R. H. *Coord. Chem. Rev.* **1995**, *144*, 1−38. (d) Yachandra, V. K.; Sauer, K.; Klein, M. P. *Chem. Rev.* **1996**, *96*, 2927−2950.

(13) (a) Bhaduri, S.; Tasiopoulos, A. J.; Bolcar, M. A.; Abboud, K. A.; Streib, W. E.; Christou, G. *Inorg. Chem.* **2003**, *42*, 1483−1492. (b) Dimitrou, K.; Brown, A. D.; Christou, G.; Concolino, T. E.; Rheingold, A. L. *Chem. Commun.* **2001**, *37*, 1284−1285. (c) Reddy, K. R.; Rajasekharan, M. V.; Arulsamy, N.; Hodgson, D. J. *Inorg. Chem.* **1996**, *35*, 2283−2286.

(14) (a) Nugent, J. *Biochim. Biophys. Acta* **2001**, *1503*, 1−123. (b) Ding, Z. Y.; Li, L.; Wade, D.; Gloyna, E. F. *Ind. Eng. Chem. Res.* **1998**, *37*, 1707−1716. (c) Reddy, K. R.; Rajasekharan, M. V.; Padhye, S.; Dahan, F.; Tuchagues, J. P. *Inorg. Chem.* **1994**, *33*, 428−433. (d) Snider, B. B. *Chem. Rev.* **1996**, *96*, 339−364.

(15) (a) Nair, V.; Mathew, J.; Prabhakaran, J. *Chem. Soc. Rev.* **1997**, *26*, 127−132. (b) Cao, H.; Suib, S. L. *J. Am. Chem. Soc.* **1994**, *116*, 5334−5342. (c) Trovarelli, A. *Catal. Rev.* **1996**, *38*, 439−520. (d) Matatov-Meytal, Y. I.; Sheintuch, M. *Ind. Eng. Chem. Res.* **1998**, *37*, 309−326.

(16) (a) Imamura, S.; Doi, A.; Ishida, S. *Ind. Eng. Chem. Prod. Res. Dev.* **1985**, *24*, 75−80. (b) Hamoudi, S.; Belkacemi, K.; Sayari, A.; Larachi, F. *Chem. Eng. Sci.* **2001**, *56*, 1275−1283. (c) Hamoudi, S.; Belkacemi, K.; Larachi, F. *Chem. Eng. Sci.* **1999**, *54*, 3569−3576. (d) Ding, Z. Y.; Frisch, M. A.; Li, L.; Gloyna, E. F. *Ind. Eng. Chem. Res.* **1996**, *35*, 3257−3279.

(17) Tasiopoulos, A. J.; Abboud, K. A.; Christou, G. *Chem. Commun.* **2003**, *39*, 580−581.

(18) Arndt, D. *Manganese Compounds as Oxidizing Agents in Organic Chemistry;* Open Court Publishing Company: Illinois, USA, 1981.

(19) Qi, G. S.; Yang, R. T. *Chem. Commun.* **2003**, *39*, 848−849.

(20) Maayan, G.; Christou, G. *Inorg. Chem.* **2011**, *50*, 7015−7021.

(21) (a) Lin, X.; Doble, D. M. J.; Blake, A. J.; Harrison, A.; Wilson, C.; Schroeder, M. *J. Am. Chem. Soc.* **2003**, *125*, 9476−9483. (b) Mills, A. M.; Ruck, M. *Inorg. Chem.* **2006**, *45*, 5172−5178.

(22) (a) Lis, T. *Acta Crystallogr., Sect. B* **1980**, *B36*, 2042−2046. (b) Boskovic, C.; Huffman, J. C.; Christou, G. *Chem. Commun.* **2002**, *38*, 2502−2503.

(23) van der Sluis, P.; Spek, A. L. *Acta Crystallogr.* **1990**, *A46*, 194−201.

(24) Spek, A. L. *Acta Crystallogr.* **1990**, *A46*, C34−C36.

(25) *SHELXTL6;* Bruker-AXS: Madison, WI, 2000.

(26) (a) Tasiopoulos, A. J.; Mishra, A.; Christou, G. *Polyhedron* **2007**, *26*, 2183−2188. (b) Mishra, A.; Tasiopoulos, A. J.; Wernsdorfer, W.; Moushi, E. E.; Moulton, B.; Zaworotko, M. J.; Abboud, K. A.; Christou, G. *Inorg. Chem.* **2008**, *47*, 4832−4843.

(27) Papatriantafyllopoulou, C.; Abboud, K. A.; Christou, G. *Polyhedron* **2013**, *52*, 196−206.

(28) (a) Liu, W.; Thorp, H. H. *Inorg. Chem.* **1993**, *32*, 4102−4105. (b) Roulhac, P. L.; Palenik, G. J. *Inorg. Chem.* **2003**, *42*, 118−120.

(29) (a) Mereacre, V.; Ako, A. M.; Akhtar, M. N.; Lindemann, A.; Anson, C. E.; Powell, A. K. *Helv. Chim. Acta* **2009**, *92*, 2507−2524.

(b) Romanenko, G. V.; Fursova, E. Yu.; Ovcharenko, V. I. *Russ. Chem. Bull., Int. Ed.* **2009**, *58*, 1−10.
(30) See Supporting Information.
(31) Milios, C. J.; Wood, P. A.; Parsons, S.; Foguet-Albiol, D.; Lampropoulos, C.; Christou, G.; Perlepes, S. P.; Brechin, E. K. *Inorg. Chim. Acta* **2007**, *360*, 3932−3940.
(32) (a) O'Connor, C. J. *Prog. Inorg. Chem.* **1982**, *29*, 203−283. (b) Vleck, J. H. V. *The Theory of Electric and Magnetic Susceptibilities;* Oxford University Press: London, U.K., 1932.
(33) (a) Plaksin, P. M.; Stoufer, R. C.; Mathew, M.; Palenik, G. J. *J. Am. Chem. Soc.* **1972**, *94*, 2121−2122. (b) Stamatatos, T. C.; Christou, G. *Philos. Trans. R. Soc. London* **2008**, *366*, 113−125.
(34) Wieghardt, K.; Bossek, U.; Bonvoisin, J.; Beauvillain, V.; Girerd, J.-J.; Nuber, B.; Weiss, J.; Heinze, J. *Angew. Chem., Int. Ed. Engl.* **1986**, *25*, 1030−1031.
(35) Kahn, O. *Molecular Magnetism;* VCH: New York, 1993.
(36) Vincent, J. B.; Tsai, H.-L.; Blackman, A. G.; Wang, S.; Boyd, P. D. W.; Folting, K.; Huffman, J. C.; Lobkovsky, E. B.; Hendrickson, D. N.; Christou, G. *J. Am. Chem. Soc.* **1993**, *115*, 12353−12361.
(37) Stoll, S.; Schweiger, A. *J. Magn. Reson.* **2006**, *178*, 42−55.
(38) Policar, C.; Knupling, M.; Frapart, Y. M.; Un, S. *J. Phys. Chem. B* **1998**, *102*, 10391−10398.
(39) Cooper, S. R.; Dismukes, G. C.; Klein, M. P.; Calvin, M. *J. Am. Chem. Soc.* **1978**, *100*, 7248−7252.
(40) Stebler, M.; Ludi, A.; Buergi, H.-B. *Inorg. Chem.* **1986**, *25*, 4743−4750.
(41) Carlson, K. D.; Geiser, U.; Kini, A. M.; Wang, H. H.; Montgomery, L. K.; Kwok, W. K.; Beno, M. A.; Williams, J. M.; Cariss, C. S.; Crabtree, G. W.; Whangbo, M. H.; Evain, M. *Inorg. Chem.* **1988**, *27*, 965−967.
(42) Glerup, J.; Goodson, P. A.; Hazell, A.; Hazell, R.; Hodgson, D. J.; McKenzie, C. J.; Michelsen, K.; Rychlewska, U.; Toftlund, H. *Inorg. Chem.* **1994**, *33*, 4105−4111.
(43) Frapart, Y. M.; Boussac, A.; Albach, R.; AnxolabehereMallart, E.; Delroisse, M.; Verlhac, J. B.; Blondin, G.; Girerd, J. J.; Guilhem, J.; Cesario, M.; Rutherford, A. W.; Lexa, D. *J. Am. Chem. Soc.* **1996**, *118*, 2669−2678.
(44) Goodson, P. A.; Glerup, J.; Hodgson, D. J.; Michelsen, K.; Pedersen, E. *Inorg. Chem.* **1990**, *29*, 503−508.
(45) Oki, A. R.; Glerup, J.; Hodgson, D. J. *Inorg. Chem.* **1990**, *29*, 2435−2441.
(46) Suzuki, M.; Senda, H.; Kobayashi, Y.; Oshio, H.; Uehara, A. *Chem. Lett.* **1988**, 1763−1766.